EI SEVIER

Contents lists available at ScienceDirect

## Journal of Volcanology and Geothermal Research

journal homepage: www.elsevier.com/locate/jvolgeores



# Lava-water interaction and hydrothermal activity within the 2014–2015 Holuhraun Lava Flow Field, Iceland



Colin M. Dundas <sup>a,\*</sup>, Laszlo Keszthelyi <sup>a</sup>, Einat Lev <sup>b</sup>, M. Elise Rumpf <sup>a</sup>, Christopher W. Hamilton <sup>c</sup>, Ármann Höskuldsson <sup>d</sup>, Thorvaldur Thordarson <sup>e</sup>

- <sup>a</sup> U.S. Geological Survey, Astrogeology Science Center, 2255 N. Gemini Dr., Flagstaff, AZ 86001, USA
- <sup>b</sup> Lamont-Doherty Earth Observatory, Columbia University, 61 Route 9W, Palisades, NY 10964, USA
- <sup>c</sup> Lunar and Planetary Laboratory, University of Arizona, 1629 E. University Blvd., Tucson, AZ 85721, USA
- <sup>d</sup> Nordic Volcanological Center, Institute of Earth Sciences, University of Iceland, Sturlugata 7, 101 Reykjavik, Iceland
- <sup>e</sup> Faculty of Earth Sciences, University of Iceland, Sturlugata 7, 101 Reykjavik, Iceland

#### ARTICLE INFO

#### Article history: Received 29 May 2020 Received in revised form 22 October 2020 Accepted 23 October 2020 Available online 26 October 2020

#### ABSTRACT

Lava that erupted during the 2014–2015 Holuhraun eruption in Iceland flowed into a proglacial river system, resulting in aqueous cooling of the lava and an ephemeral hydrothermal system. We carried out a monitoring study of this system from 2015 to 2018 to document the cooling of the lava over this time, using thermocouple measurements and data-logging sensors. The heat loss rate from advection through this hydrothermal system in August 2015 was  $\sim 5.5 \times 10^8$  W; since eruption, aqueous cooling likely accounted for  $\sim 1\%$  of the total heat loss from the lava. This estimate excludes steam losses from fumaroles as well as any groundwater that was not released to the surface, and thus is a lower bound. Near the terminus of the flow, advection of heat by flowing water may have locally accounted for tens of percent of the total cooling of that part of the flow. Our data quantify the importance of water cooling for this lava flow and can be compared with models to better understand lavawater interactions more generally. We also provide detailed methods for simple, low-cost monitoring of similar instances in the future.

Published by Elsevier B.V.

#### 1. Introduction

Cooling is a fundamental factor in the evolution of lava flows and is one of the major controls on their length and behavior. Cooling in a dry setting is relatively well studied and modeled (e.g., Hon et al., 1994: Keszthelvi and Denlinger, 1996: Fagents and Greelev, 2001: Harris and Rowland, 2001; Keszthelyi et al., 2003; Patrick et al., 2004; Rumpf et al., 2013). However, water plays an important role in the cooling of many lava flows and the creation of distinctive volcanic features. For instance, aqueous cooling is associated with the formation of features such as hackly and columnar jointing (e.g., the lava entablatures and colonnades described by Sæmundsson (1970) and Long and Wood (1986)). The latter requires advective heat transport to produce a constant cooling rate (e.g., Goehring and Morris, 2008). Other features produced by various forms of lava-water interaction include rootless cones (e.g., Thorarinsson, 1953; Fagents and Thordarson, 2007; Hamilton et al., 2017), maars (e.g., Lorenz, 1973), tuff rings and cones (e.g., Sheridan and Wohletz, 1983), pillow lavas, and volcaniclastics such as hyaloclastites and peperites (e.g., Skilling et al., 2002). Water

cooling has also been proposed to explain temperature profiles within lava lakes or ponds and around small sills that are inconsistent with simple conduction (e.g., Hardee, 1980, 1982; Baker et al., 2015). Widespread evidence for lava—water interaction has been reported on Mars (e.g., Squyres et al., 1987; Greeley and Fagents, 2001; Lanagan et al., 2001; Milazzo et al., 2009; Hamilton et al., 2010, 2011) and understanding these interactions is thus important to both the volcanic and aqueous history of that planet, two topics of high scientific interest (MEPAG, 2020). However, lava—water interactions are challenging to model and suffer from a scarcity of quantitative field data on aqueous cooling of lavas. Here, we report on a series of experiments we conducted to collect in situ data that record the effects and evolution of recent lava—water interactions in Iceland.

The 2014–2015 eruption at Holuhraun in Iceland (Fig. 1) provides an excellent example of one style of lava–water interaction: lava entering a river system. Pedersen et al. (2017) provide an overview of the emplacement and evolution of the lava, and thus we provide only a brief review here. The precursor to the eruption was northward-propagating seismicity that initiated about 5 km east of the Bárðarbunga central volcano before eruptive fissures opened to the north of the Vatnajökull ice cap (e.g., Sigmundsson et al., 2015). A total of approximately 1.44 km³ of basaltic lava (1.21 km³ dense rock equivalent; Bonny et al., 2018) was

<sup>\*</sup> Corresponding author.

E-mail address: cdundas@usgs.gov (C.M. Dundas).

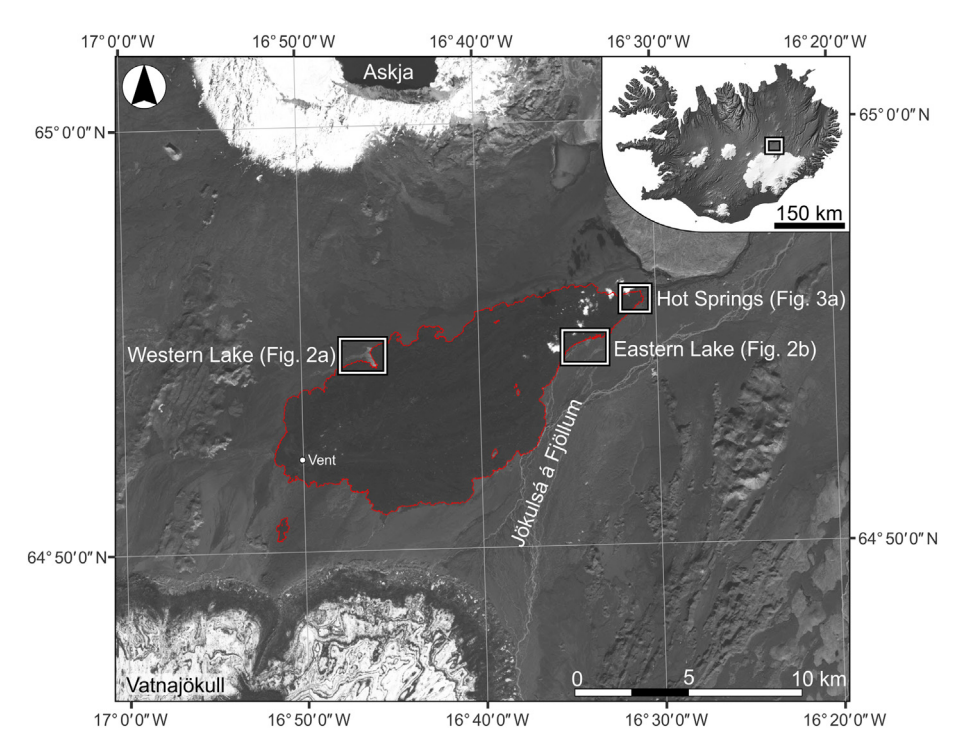


Fig. 1. Context image showing the location of the 2014–2015 Holuhraun lava flow field (outlined in red) as well as the position its main source vent and the locations of Fig. 2a (western lake), Fig. 2b (eastern lake, shown in Fig. 4), and Fig. 3 (hot springs, located at the lava terminus). Seismicity leading to the eruption initiated at the Bárðarbunga central volcano southwest of this figure. The box within the inset map of Iceland shows the location of the study area in the highlands, north of the Vatnajökull ice cap. The background is a part of a Landsat 8 image (Band 8) acquired on September 25, 2019 (LC08\_L1TP\_217015\_20150925\_20170403\_01\_T1\_B8).

erupted between August 31, 2014 and February 27, 2015, with a peak effusion rate of at least 350 m³/s and flows that reached as far as 17 km from the vent (Fig. 1). The lava ultimately covered approximately 84 km² (Pedersen et al., 2017). The pre-eruption temperature of the lava was estimated to be 1181–1191 °C, close to the liquidus temperature of approximately 1195 °C (Kolzenburg et al., 2017). Thermocouple and Forward Looking Infrared Radiometer (FLIR) camera measurements 4.3 km from the vent show that the lava cooled to 1080–1130 °C (mean 1095 °C) during transport before stopping (Kolzenburg et al., 2017). The lava flow field is a mix of spiny and rubbly pāhoehoe, with some 'a'ā (Pedersen et al., 2017). It was the largest eruption in Iceland since the Laki (Skaftá Fires) eruption of 1783–1784 (cf. Thordarson and Self, 1993).

The lava was emplaced on the sand and gravel of the floodplain and braided channel system of the Jökulsá á Fjöllum river, which emanates from the Dyngjujökull outlet glacier of the Vatnajökull ice cap (Fig. 1). The lava intersected the river system and followed the course of the channel, providing ample opportunity for lava–water interactions. These interactions were largely non-explosive (Pedersen et al., 2017). Water was heated where the lava flowed over wet ground, and groundwater continued to flow beneath the lava. The system is somewhat analogous to the aqueous cooling of the "Valley of Ten Thousand Smokes" ignimbrite produced by the Novarupta–Katmai eruption of 1912 (Hildreth and Fierstein, 2012), but smaller in size, lower in energy and created by lava rather than volcanic ash. Bonnefoy et al. (2019) provided some observations of the hydrology and water fluxes from the Holuhraun flow field, which are controlled by groundwater and surface runoff and their interactions with the hot lava core.

## 2. Observations

## 2.1. Site description and study overview

This study uses field observations and in situ sensor data to record the evolution of the lava-heated hydrological system. We were only able to make brief site visits during the prolonged cooling of the flow field, but iteratively developed a continuous monitoring network. Our initial reconnaissance in 2015 documented the conditions approximately six months after the end of the eruption, but at that time we were not equipped to set up longer-term monitoring. We returned in 2016 and emplaced several long-lived sensors. Data were collected from these sensors in 2017, when they were replaced, improved, and augmented. All sensors were finally removed in 2018 when the system had largely cooled to ambient conditions. These data allow us to demonstrate the significant added value of continuous, as opposed to intermittent, monitoring of the hydrological system. Establishing a sensor network in the relatively inaccessible and highly dynamic environment of a lava flow emplaced into a major river proved to be a substantial technical challenge. One of the main outcomes of this work is a set of protocols and lessons learned for future attempts to monitor similar fluvio-volcanic interactions.

The local hydrology around the flow field includes distributed groundwater-fed springs and seeps as well as glacially fed streams. These waters reach and dive under the lava both near the vent at the western edge of the flow (Figs. 1, 2a, c), and along the southern/eastern margin (Fig. 2b, d). The river was initially dammed by the southern margin of the lava, forcing surface water into and beneath the lava and forming a transient lake beside the flow. Heated water exited from warm springs issuing from several locations beneath the distal end of the lava and fed into the existing braided river channel. These springs, and emergent groundwater just northeast of the lavas, were the main surface water sources for the river at the toe of the flow field in 2015. Steam plumes were observed rising from the interior of the flow field, but their flux was not quantified. One key question that we sought to answer was whether the flux of surface water into the lava was similar to the spring outflow or if more complex groundwater processes were taking place.

Conditions were markedly different in 2016–2018, when the stream flowing along the southern edge of the lava reached all the way to the

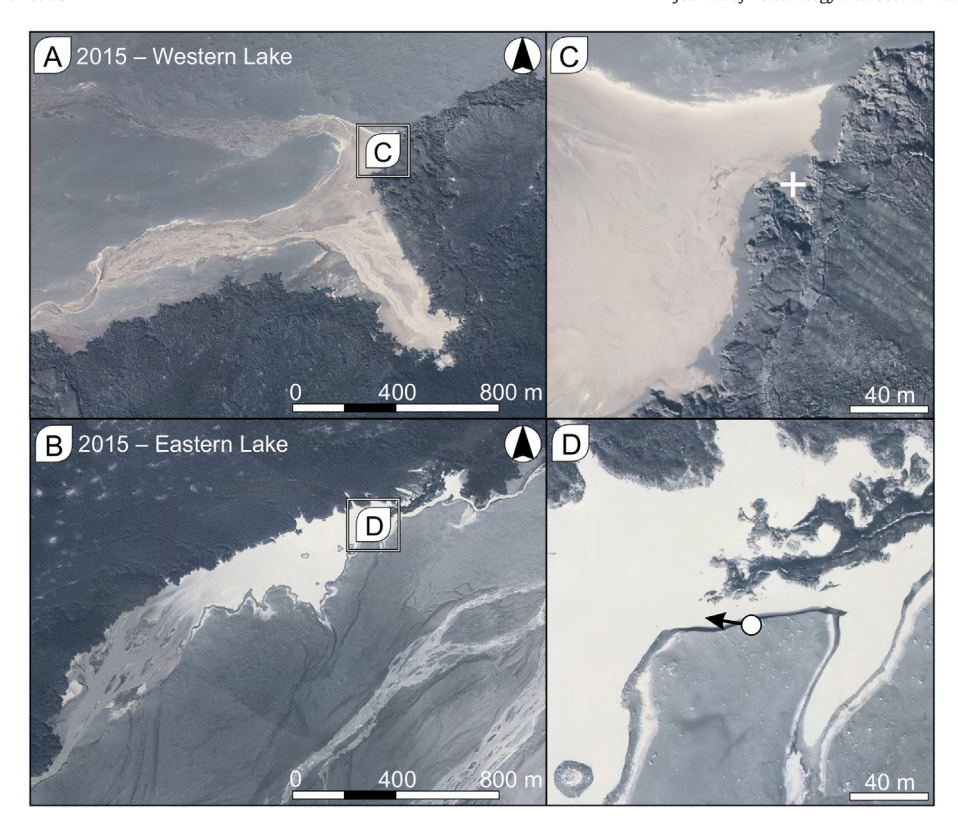


**Fig. 2.** (A) and (B) show the locations of the western and eastern lava-dammed lakes, respectively, as well as the in locations of the insets shown in panels (C) and (D). The cross in (C) shows the location of the stream gage sensor deployed in 2017. The circle in (D) shows the location of the field photographs shown in Fig. 5, and the arrow indicates the camera look direction. The basemap image (20 cm/pixel) is a part of an UltraCam orthomosaic acquired by IsViews on September 6, 2015.

northeast end of the flow field. This change is ascribed to the breaching of a sediment dam in July 2016 (Bonnefoy et al., 2019). Outflow from the springs at the lava terminus continued but cooled over time, and by July 2018 spring temperatures were so near ambient conditions that we could no longer reliably measure the hydrothermal heating. The one area that did not significantly change over the three years was the network of groundwater-fed streams just north of the lava terminus. The reader is referred to Bonnefoy et al. (2019) for additional details on the history of the hydrologic system and associated landscape evolution at the 2014–2015 Holuhraun lava flow field.

## 2.2. Documenting cooling by water

In the 2015 reconnaissance, water temperatures were only obtained as spot measurements using a K-type thermocouple. Water fluxes, however, were investigated in detail. Velocity estimates were made across all heated streams using video footage of multiple floating objects passing known distances. Objects were thrown at various locations across the width of the stream to determine an average value. We used two independent feature-tracking approaches to estimate velocity given the viewing geometry and scale information in the scene. Stream depth profiles with 1-m spacing were made at the same locations as the velocity estimates. This enabled us to calculate the water flux at each location. Combined with temperature measurements, this enabled our best estimate for the excess heat carried by the water as a result of heating from the lava in 2015.

In 2016 through 2018, we used several types of data-logging sensors to collect continuous records of water depth and temperature, as well as environmental conditions. The earlier parts of the dataset proved to be too sparse spatially to monitor the total heat transport. By the time the network was improved in 2017, temperatures were only minimally above background. Nevertheless, the data recorded key behavior on

seasonal and diurnal timescales that are important to interpreting the cooling of the system. We used three types of sensors: (1) Omega Engineering® OMYL-RH23 loggers for atmospheric temperature, pressure and relative humidity; (2) Omega Engineering® OM-CP-MICROTEMP submersible temperature sensors: and (3) Onset® HOBO® U20 submersible temperature and pressure sensors. For brevity, we refer to these as weather, temperature, and P-T sensors, respectively. The data used herein are available (Dundas et al., 2020). The key requirements for the sensors were that they be small, lightweight, function in freezing conditions, and operate on battery power for over a year. Most of these requirements were driven by the fact that the key sites are only accessible on foot over challenging terrain. All the hardware for the entire network needed to fit in a backpack. Additionally, the dynamic nature of the system favored a flexible deployment strategy. Because the region is a national park, it was also important that the instruments have minimal visual impact and not damage the environment. These considerations ruled out traditional gaging stations favored by the U.S. Geological Survey for monitoring water flow (Sauer and Turnipseed, 2010; Turnipseed and Sauer, 2010). Similarly, even compact telemetry stations were too bulky and visible to utilize in this setting. The side benefit of the need to use a minimum of hardware was that the costs were very modest (~\$1000 per site). Additional details of sensor installation and associated challenges are discussed in the Appendix.

#### 2.3. 2015 reconnaissance observations

The bulk of our reconnaissance observations were similar to those reported by Bonnefoy et al. (2019) from the area around the lava terminus where notable warm springs were well established. A detailed view of this area shows the mix of rubbly and spiny pāhoehoe that filled the existing river channel (Fig. 3). Our 2015 observations were obtained on August 21, 23–25, and 27, and the site was revisited on September 4.

Water heated to ~30–50 °C emerged at multiple discrete sources over an ~350-m-wide flow front. The water emerging from the central section of thicker rubbly pāhoehoe was notably warmer than that flowing from the thinner and more lateral spiny pāhoehoe lobes. Unheated water from cold streams that flowed along the northern side of the lava flow mixed with the heated water across the braided river deposits. The efflux from the hot springs and resulting level of the streams showed minimal visible variation over time during this visit, but the quantity of water flowing in from the cold side streams was substantially higher on August 24–25.

A stream flowed along much of the distal ~15 km of the southeast side of the lava flow field. This region was visited on August 23–25, 2015. On August 23, a shallow braided stream was flowing into the side of the lava at multiple locations (Fig. 4a) 2–3 km up-flow from the terminus. No surface water reached the terminus of the lava flow field. The lava at the region where this southern stream ended had a thin silt coating, indicating the high-water mark of a previous lake 2–3 m above the water surface, and a broad shallow basin alongside the lava showed traces of a recent lake (Fig. 4a). On August 24, the lake basin had been reoccupied to ~1.5 m below the high-water mark and was draining into the permeable rubbly lava (Fig. 4b). A series of pools extended into the lava, connected via the extreme porosity of the fragmented surface.

We made profiles of this southern stream near where it flowed under the lava on August 23 (near the lake terminus) and August 24 (roughly 1 km farther upstream), by measuring depths at regular intervals, and made estimates of the stream velocity. The stream flux roughly doubled overnight (8  $\pm$  3 m<sup>3</sup>/s on the 23rd versus 16  $\pm$  4 m<sup>3</sup>/s on the 24th). Profiles of the spring-fed outlet streams at the lava terminus (Fig. 3b) were also measured, crossing each of the major branches of the braided system, and used to construct an estimate of the water flux from the terminus. Based on the stream profile measurements, the total output of the toe springs was  $4.9 \pm 1.1 \text{ m}^3/\text{s}$  suggesting that during the few days of observations in August 2015 the influx of water into the lava flow field was 2-3 times larger than the surface outflow. What we could not determine definitively from these reconnaissance observations was whether the difference was lost as steam or to subsurface flow or if we were observing a temporary increase in the streamflow coming to the lava. Both factors were likely involved to some extent but the latter was almost certainly important given the rise in lake level.

Temperatures were measured at selected points along the profiles of the outflow streams. In conducting vertical temperature profiles, we observed a few degrees Celsius cooling of the surface of the warm streams. Temperatures a few centimeters deep in the sand-and-gravel substrate were near ambient, as much as 21  $^{\circ}\text{C}$  cooler than the flowing water. The temperature may have been even cooler because warm water may have accompanied the thermocouple during insertion into the sediment. This suggests flow of unheated or minimally heated water through the streambed.

We also systematically sampled the temperatures of many of the springs emerging from the toe of the flow on August 21 and August 24, immediately upstream from the stream profiles, but it was not practical to make water flux measurements at those locations due to their distributed nature and complex topography. We briefly revisited the hot springs on August 27. During the three days of our observations neither the level of the outflow streams nor the temperature of the outflows visibly varied. This was despite the dramatic changes to the streamflow into the lava only 2–3 km away.

In the upstream region of the lake and feeder stream, we made temperature measurements to establish the baseline temperature of near-surface water, which was approximately 9–10 °C. Subsequent observations (section 2.4.2) suggest that these values represent afternoon peaks rising from a baseline temperature of 5–6 °C. Some cold springs and feeder streams north of the flow were colder (4 °C) than this baseline value. Snow buried by sand was observed to survive in late August at some locations along the flow field margin, indicating that subsurface temperatures are generally not far above freezing.

## 2.4. 2016-2018 monitoring

## 2.4.1. 2016-2017

To track the cooling of the system, we revisited the site on several occasions between August 2016 and July 2018, and emplaced long-lived sensors at several locations. We were especially interested in recording the response of the warm springs to diurnal, seasonal, and inter-annual variations of the input of cold water. Limited numbers of available sensors meant that the dataset that we collected was not as extensive as desired. In 2016, the sensor distribution (Fig. 5) was as follows: one P–T sensor in the warmest remaining spring near the lava terminus ("Toe Spring"); one P–T sensor in a pool along the northern edge of the lava ("Side Pool"); one temperature sensor in a warm spring feeding

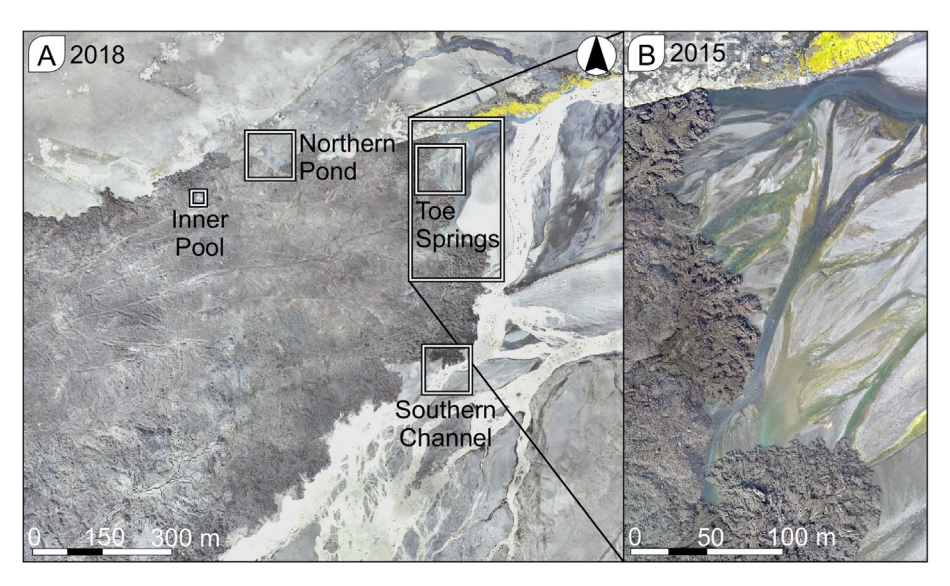


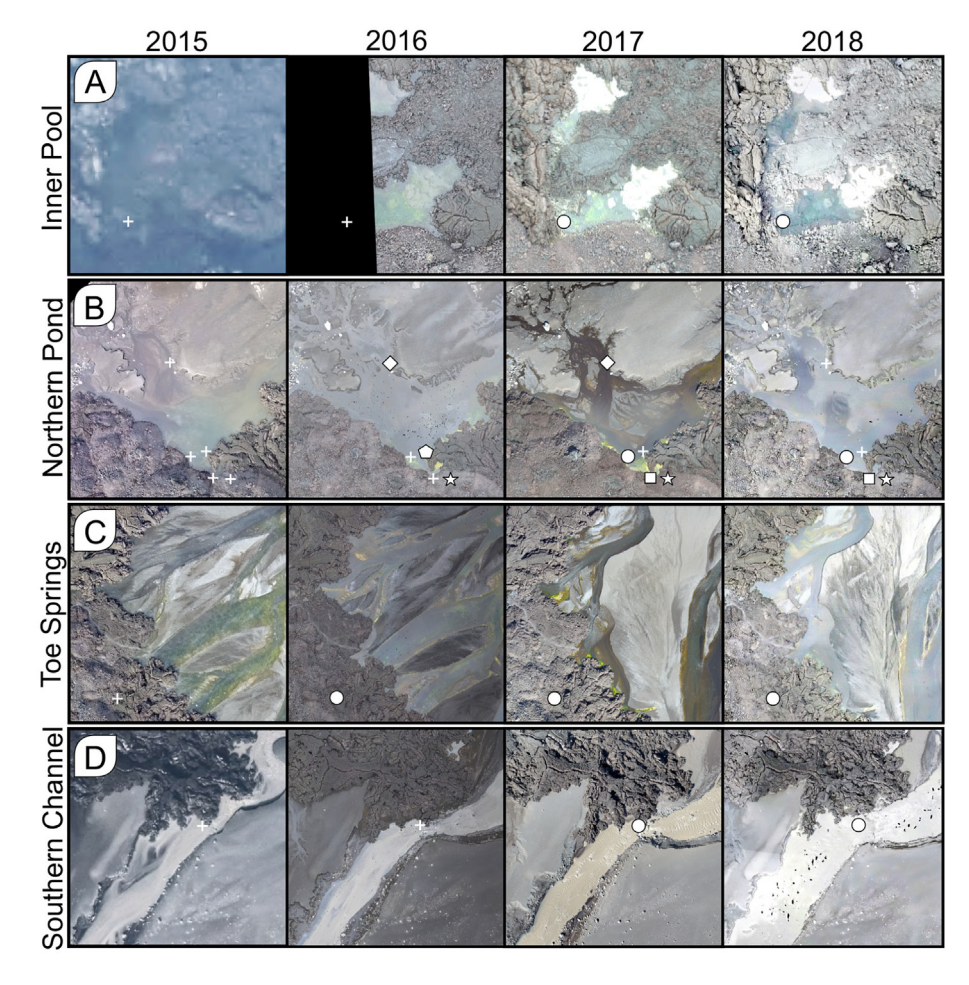
Fig. 3. (A) Locations of the key study locations in the Hot Springs region, including the Inner Pool (Fig. 5a), Northern Pond (Fig. 5b), Toe Springs (Fig. 5c), and Southern Channel (Fig. 5d). The basemap image is a 4 cm/pixel orthomosaic generated from Trimble UX5-HP small Unmanned Aerial System (sUAS) data acquired on August 3, 2018. (B) A magnified view of the Toe Springs region on September 4, 2015. The 4 cm/pixel orthomosaic shown in (B) was generated from DJI Phantom 3 Pro sUAS data. See Scheidt and Hamilton (2019) for sUAS data specifications.



Fig. 4. Transient lake location looking approximately west along the southern margin of the lava, observed in August 2015. (A) On August 23, 2015 the stream flowed along the lava margin before disappearing into the rubble at right. Note old high-water mark on the lava caused by a thin coating of mud. (B) On August 24, 2015 the lake had been refilled to near the former high-water mark. White arrows indicate two corresponding features in the images for reference. Note person for scale (blue arrow). See Fig. 2d for location. Photo credit: U.S. Geological Survey.

into the side pool ("Warm Spring"); one temperature sensor in a shallow groundwater-fed stream feeding into the side pool ("Cold Stream"); and one weather sensor concealed in lava rubble just above the side pool to provide atmospheric information. The lake along the southern

margin of the lava that had shown interesting dynamics in 2015 was not instrumented because the stream breaking through the sediment dam in July 2016 (Bonnefoy et al., 2019) had altered the dynamics along that margin of the flow.



**Fig. 5.** Time-series view of the four locations shown in Fig. 3a. In 2015, panel (A) shows a 20 cm/pixel UltraCam view of the Inner Pool (acquired on September 6, 2015), whereas panels (B), (C), and (D) show 4 cm/pixel DJI Phantom 3 Pro sUAS views of the Northern Pond, Toe Springs, and Southern Channel, respectively (acquired on September 4, 2015). In 2016, panels show 1 cm/pixel views of same locations imaged using a Trimble UX5-HP sUAS on July 28, 2016. In 2017, panels show 2.3 cm/pixel views acquired using a DJI Phantom 4 Pro sUAS on July 25–28, 2017. In 2018, panels show 4 cm/pixel views acquired by a Trimble UX5-HP sUAS on August 3, 2018. For more detail and for access to the sUAS data see Scheidt and Hamilton (2019). Circles show the locations of sensors that were deployed in a given year; however, in panel (B) the pentagon shows the location of the sensors deployed in the Side Pool (deployed in 2016, but lost before recovery in 2017); the diamonds identify the location of sensors placed within the Cold Stream (2016–2017); the squares show the location of the Warm Spring (2016–2017); the circles show the location of the second Side Pool sensor (2017–2018); and the stars identify the location of the weather sensor (2016–2018). Crosses show the corresponding locations of the sensors in years when the sensors were not deployed.

Measurements were downloaded from these sensors in September 2016 and July 2017, with several difficulties. The most important issue was that the thin cable holding the Side Pool sensor rusted through sometime after September 2016 causing the sensor to break loose and be lost. When we installed the sensor, the site seemed to be in a lowenergy environment. However, substantial fluvial sediment transport and deposition occurred between our 2016 and 2017 visits, demonstrating the need to anchor sensors more robustly. The atmospheric pressure sensor produced obviously inaccurate data (reported pressures exceeded sea-level values), and thus accurate corrections to invert P-T sensor pressure data for water depth were not possible; we attempted to derive a correction factor by comparison with an accurate sensor, but these data were not consistent with any unique scaling. The Cold Stream sensor was found buried beneath a few centimeters of sand on both occasions of data collection, and thus did not directly measure water temperature. The stream was too shallow to avoid this issue; thus, we abandoned attempts to monitor streams that were only a few centimeters deep.

## 2.4.2. 2017-2018

Several steps were taken to improve the network that we deployed in 2017 (Fig. 5), and due to concerns about battery life in harsh conditions, the 2016 sensors were removed. One P–T data logger was placed in the toe spring at the precise location of the previous sensor. Another was placed in the side pool location, several meters from the former location in a site more protected from currents and sediment transport. A third P–T sensor was placed in a warm pool entirely surrounded by lava ("Inner Pool"), and a fourth was placed in the glacial stream at the southern edge of the flow terminus. A final P–T sensor was placed at the edge of a shallow ephemeral lake on the northern edge of the flow, ~10 km from the other sensors near the terminus, to understand the water input upstream. The weather sensor was also replaced at the previous location.

The data collected from this network for the 2017–2018 interval were of significantly better quality than our initial (2016–2017) attempt. Water depths were successfully retrieved from pressures by correcting for atmospheric pressure variations recorded by the weather sensor data. The stream bottoms were irregular and the sensors were not resting on the bottom, but the changes in depth rather than the absolute values are the main quantity of interest here. The only major issue in the data from these sensors was that the lake sensor was buried by more than half a meter of sediment, which filled the polyvinyl chloride (PVC) pipe housing with silt and resulted in inaccurate water depth values.

## 2.4.3. Summary of observations

Figs. 6 and 7 show the data from these sensors (Figs. 6–7) and some representative thermocouple measurements from the same locations at times when no sensor was present. The full datasets, as well as Global Positioning System (GPS) coordinates and more information on the emplacement and known issues of each sensor, are available in Dundas et al. (2020).

During 2016–2017, the Toe Spring temperature initially decreased, then rose to, and fell from, a new peak in November 2016. This variation occurred in the months after the southern stream broke through the sediment dam in July 2016 (Bonnefoy et al., 2019). The temperature dropped smoothly and monotonically from this peak until the end of our monitoring campaign in 2018. The Warm Spring and Side Pool temperatures showed a similar pattern in autumn 2016, but with different times of peak temperature. Water levels at the Warm Spring sensor dropped enough to expose it to the air (and thus much larger temperature variations) in the spring of 2017, although it remained warmer than the ambient air away from the warm pool. Cold Stream temperatures were nearly constant at slightly above freezing throughout the year. Given that the sensor was likely buried for much of this time,

this suggests that groundwater flow continued year-round even though atmospheric temperatures fell well below freezing.

Although it was not possible to correct for atmospheric pressure and determine true water depths in the 2016–2017 data, it is possible to calculate the difference in depth between the Toe Spring and Side Pool sensors for the period where both have data, because the atmospheric correction is identical. This difference reveals a change in differential depth of ~10 cm in late August 2016, where either the Toe Spring rose or the Side Pool fell in relative terms before reverting to the previous value. This does not correspond to any notable excursion in the temperature data although the Warm Spring outflow temperature (which fed the Side Pool) increased slightly.

During 2017–2018, the glacial stream on the southern edge of the lava flow field maintained a near-constant temperature of 5–6 °C (Fig. 6), with frequent warmer diurnal spikes in the summer associated with pulses of runoff. The Toe Spring continued a near-monotonic decline in temperature. The Inner Pool temperature also decayed more or less monotonically, with a drop associated with a period when the water level fell and exposed the sensor. Atmospheric pressure data from this period enabled correction of the water pressure data to derive water depths. No attempt was made to correct for different elevations, as the region is essentially flat. Water levels for both the Side Pool and Toe Spring were quite stable (Fig. 7), while the inner pool fell and then rose.

Measurements for the lake were clearly disturbed by sediment burial shortly after emplacement (Fig. S1). The pressure dataset is inaccurate due to the effects of this burial, which began not long after installation; substantially negative apparent water depths were obtained from the pressure data within two weeks of emplacement, following a period of high runoff in the glacial stream. Minor excursions to negative apparent water depth occurred even earlier but could have been due to imperfect pressure correction, because the lake was some distance from the weather sensor. However, diurnal spikes in the pressure resemble, and loosely correlate with, periods of high runoff in the glacial stream, with a longer decay time (Fig. S1) consistent with the slower loss of ponded water. The temperature record indicates that the sensor was above freezing for most of the year, falling to freezing in late April and May 2017, but because of the unknown temporal variation of depth of burial the surface conditions and water depth are uncertain.

## 3. Analysis

#### 3.1. Hydrology

One of the main questions we aimed to address was how different parts of the hydrologic system around the new lava flow field were connected. The glacially fed stream along the southern edge of the lava shows frequent pulses in water level and temperature during the summer and fall, indicating pulses in runoff (Fig. 8). Such pulses did not occur every day and are instead correlated with warm days with enhanced glacial melting. However, the correspondence is imperfect, likely because the atmospheric temperature sensor was tens of kilometers from the ice cap, which ultimately controls the hydrology. The lake along the northern margin of the lava showed similar but not identical pulses, indicating that surface flow, and synchronous recharge of the groundwater table, is largely coupled across the entire area of the lava flows.

Water levels at the Toe Spring and Side Pool varied almost imperceptibly. However, the Toe Spring, Side Pool, and Inner Pool vary in concert, but with different amplitudes (Fig. 9). Despite the low magnitude of variation, Fourier power spectra of all three also show a peak indicating a 24-h cycle (Fig. 10a), which is pronounced in the surface stream but muted in the spring/pool sensors, indicating that they are only weakly responsive to diurnal variations. Furthermore, rising water levels in all three spring/pool sensors correlate with the multi-day intervals when pulses of glacial runoff occurred (Fig. 9) and are similar to a curve of

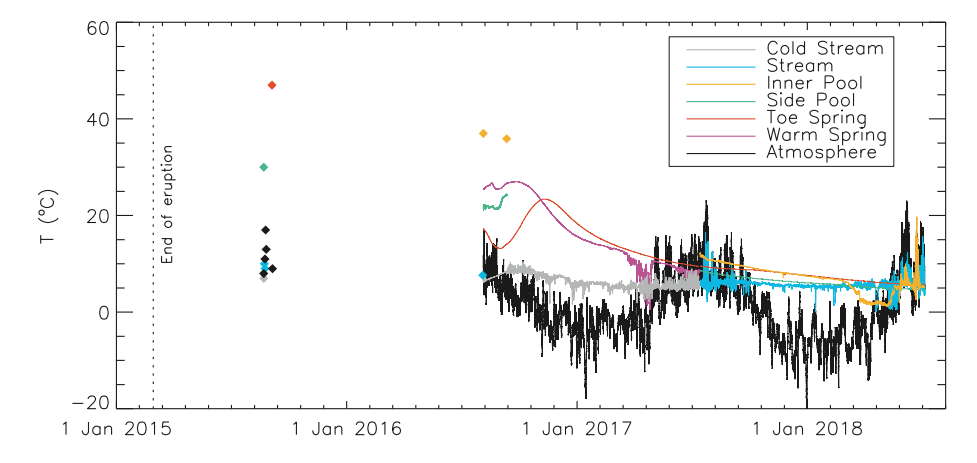


Fig. 6. Temperature data including representative thermocouple measurements from 2015 as well as monitoring from 2016 to 2018. Anomalous temperature drops in the water temperature curves are interpreted as times when the water level dropped and partially exposed the sensors to atmospheric temperature variations.

the integrated total variation in the glacial stream level. This suggests that all three water levels track the local hydraulic head (Fig. 11), which is responsive to meltwater from the glacier, increasing during periods of high melting and runoff. We did not observe convincing evidence for a phase lag between different locations. In some cases the elevated hydraulic head was likely caused by water flowing along or pooling against the side of the lava.

Fourier power spectra of temperatures (Fig. 10b) show a strong 24-h cycle for the glacial stream, while the Toe Spring and Side Pool show no such effect. The inner pool shows a weak peak indicating a diurnal temperature cycle, even when analysis is restricted to the period when the sensor was immersed. The amplitude of those diurnal temperature variations is extremely low (<1 °C); the likely reason is that water fluxes in and out of the pool were low enough that the water temperature was slightly influenced by ambient conditions, while water flowed through the Toe Spring and Side Pool more quickly.

The lack of a simple function to describe the cooling history (section 3.2) suggests that the interaction between the water and the hot lava changed modes as the hydrology evolved. The change could be related

to the breakthrough of the stream through the sediment dam along the southern margin of the lava in July 2016, perhaps leading to changes in the groundwater surface. Alternatively, there could have been some other change in the physical interactions occurring beneath the lava. The change in differential depth of the Side Pool and Toe Spring in August 2016 is consistent with an adjustment to the hydrology at around this time, as is the initially complex behavior (from July–November 2016) and subsequent monotonic cooling of the toe spring. Neither of these behaviors recurred in 2017. However, the lack of earlier monitoring data prevents a definitive answer. Bonnefoy et al. (2019) reported that groundwater table heights in the area vary from year to year, an additional factor that may influence the behavior of water beneath the lava.

#### 3.2. Water and energy fluxes

We used the 2015 data to investigate the advection of heat from the base of the lava flow. To do this, we made an estimate of the excess heat

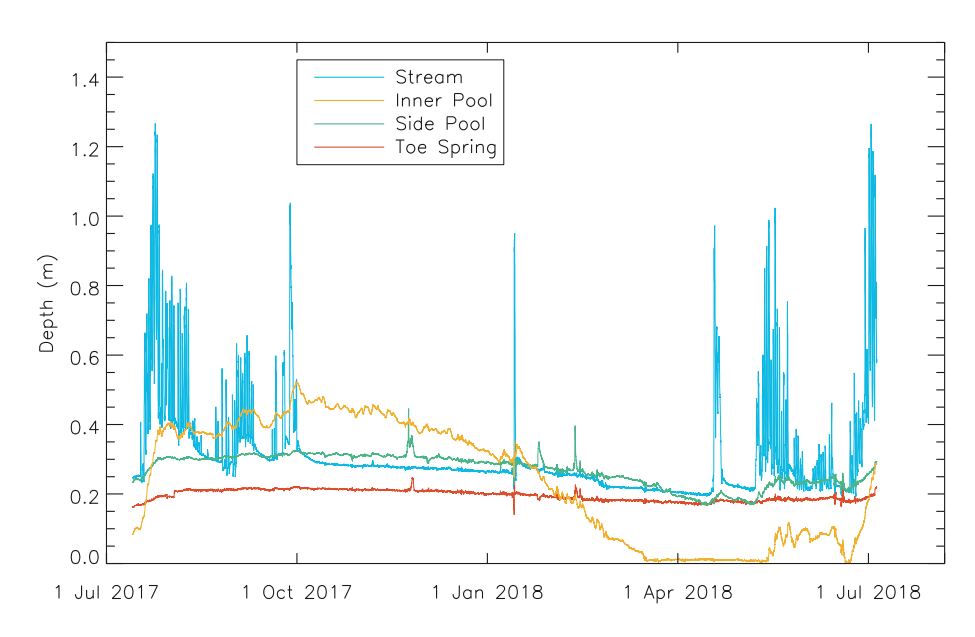


Fig. 7. Water depth measurements from July 2017 to July 2018, corrected for variations in atmospheric pressure. The stream bottoms were highly irregular and the sensors were not resting on the bottom, so the depths are relative to an arbitrary local reference (different at each location) and only relative variations are significant. The Inner Pool sensor was not immersed in early 2018 due to a low water level, which also resulted in anomalous temperatures (Fig. 4). Small (1 cm) steps early in the Toe Spring series may indicate that the sensor shifted position slightly.

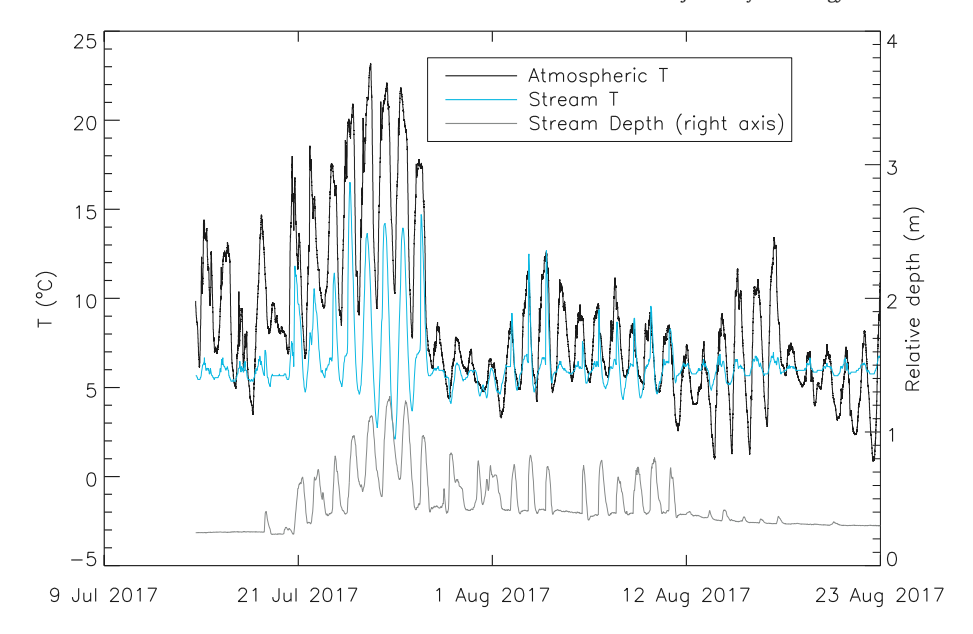


Fig. 8. Data from the glacial stream for July–August 2017. There is a distinct but imperfect visual correlation between high atmospheric temperature and high stream temperature and depth.

carried by the outflow streams using their fluxes and excess temperature above a baseline value.

For the baseline temperature of water input to the system, we used a value of 5.6 °C; this is the mean of the southern stream in the 2017–2018 data spanning 0.98 years and we assume that it was similar in 2015. This baseline value is also similar to the mean temperature of the Cold Stream groundwater north of the flow (6.3 °C) in 2016–2017 data. We use a range of  $\pm 3$  °C for error analysis, which encompasses the 3–4 °C temperatures sometimes measured in the groundwater

north of the flow at the low end and is well above all but the brief diurnal peak temperatures in the southern stream at the high end. The area-weighted temperatures and the stream velocities were used to determine the quantity of heat added to the outflowing water in 2015 (Eq. 1):

$$Q_{excess} = (X*\Delta T)*\overline{V}*\rho_{H_2O}*C_P$$

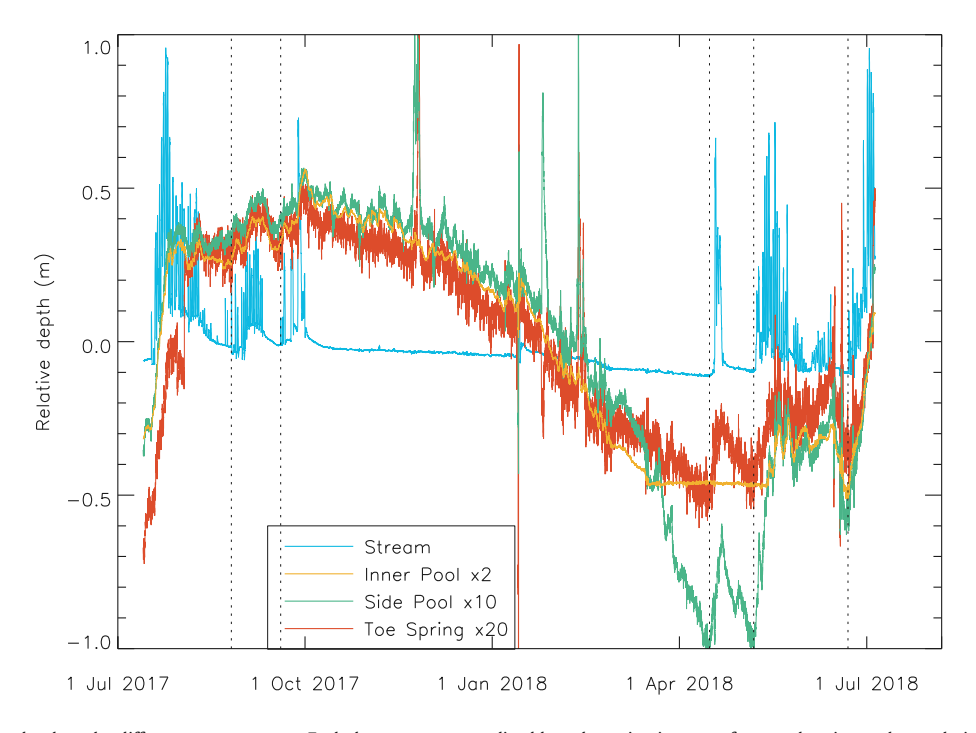
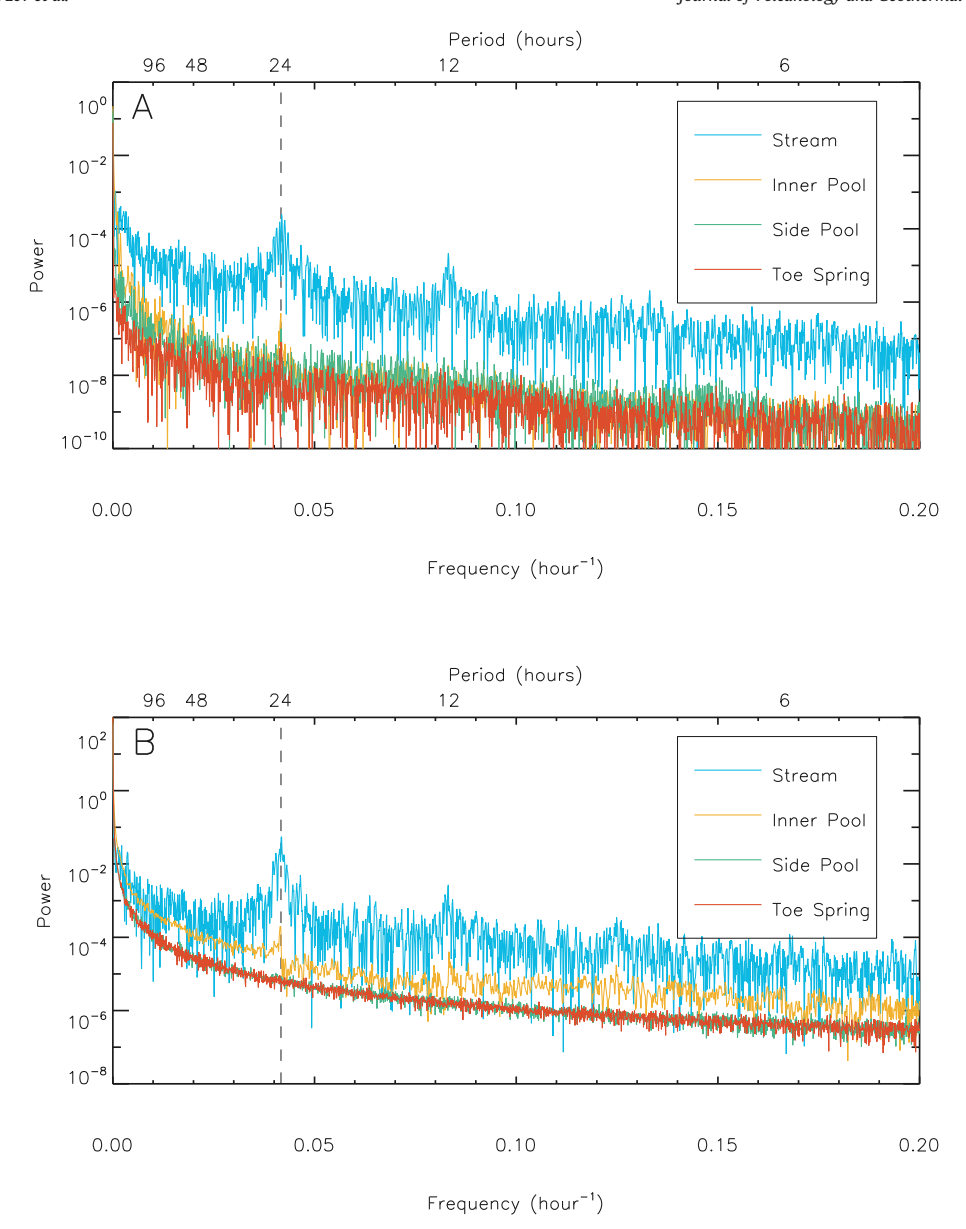
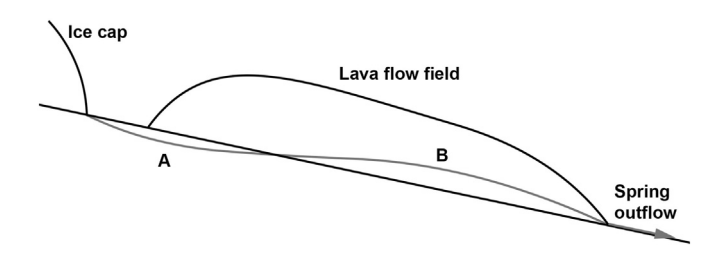


Fig. 9. Variations in relative depth at the different water sensors. Each dataset was normalized by subtracting its mean from each point to show relative variations, and arbitrary multiplicative factors were applied to show correlations better. Dividing each set by its standard deviation produced similar results. The variations in the Inner Pool, Side Pool, and Toe Spring, all fed by the hydrothermal system (the side pool is also fed by groundwater-sourced streams adjacent to the lava), are strongly correlated. These variations do not correlate with the depth of the glacial stream, but major periods of rising water in the pools and spring do correlate (vertical dashed lines indicate their onsets) with periods of strong diurnal runoff in the glacial stream.



**Fig. 10.** Fourier power spectra of the water depths (A) and temperatures (B) for multiple datasets. A) Depth variations of all of the springs and pools show a peak at a frequency corresponding to a 24-hour cycle (dashed line), although the Side Pool and Toe Spring peaks are very weak. B) Temperature variations show diurnal-cycle frequencies only in the glacial stream and the Inner Pool. Power spectra were derived using the Interactive Data Language (IDL, version 8.4.1) *fft\_powerspectrum* function. The Inner Pool series analysis used only data from the period while the sensor was immersed.



**Fig. 11.** Schematic diagram (not to scale) of the hydrology giving rise to hot springs at Holuhraun. In some areas (A) the water table does not extend into the flow but in others hydraulic head forces water into the lava (B), often associated with surface streams and/or ponding. Overland flow can also overtop the lava in places. The spring outflows occur at the lava terminus, which is the lowest-elevation surface and associated with a riverbed. Variations in the groundwater table can lead to small rises in the water depth at the outflows.

where  $Q_{excess}$  is the thermal energy added to the water, X is the channel cross-sectional area,  $\Delta T$  is the excess temperature,  $\overline{V}$  is the mean water velocity,  $\rho_{H_2O}$  is the density of water, and  $C_P$  is the specific heat of water. Values for X,  $\overline{V}$ , and  $\Delta T$  are given in Table 1. When we had multiple measurements of temperature within a stream, they were weighted by the cross-sectional area in the vicinity of the measurement.

This procedure resulted in estimates ranging from  $4.8 \times 10^8$  W to  $6.7 \times 10^8$  W with a best estimate of  $5.7 \times 10^8$  W advected from the lava in late August 2015. This is equivalent to a heat flux of ~7 W m $^{-2}$  if the relevant area is the entire lava flow. However, the heat is almost certainly derived only from a fraction of the lava area (no surface water around much of the perimeter of the flow) and thus is a stronger flux locally. An approximate lower bound on the area involved is the roughly trapezoidal area defined by the ephemeral 2015 lake and the lava terminus. This is ~2 km $^2$ , which would yield an average heat flux of ~300 W m $^{-2}$ , possibly higher within preferred pathways. Fluxes were presumably higher immediately after the eruption and diminished

towards zero over time. These fluxes are much less than the radiant heat from recently active lavas, which can remain above several thousand W  $\rm m^{-2}$  for hours after eruption (e.g., Flynn et al., 1994), but their relative importance will increase as the flows cool and develop a thick conductive crust.

We note that our heat flux values are substantially lower than those reported in Table 1 of Bonnefoy et al. (2019). This is because Bonnefoy et al. (2019) reported the total heat carried by the water as opposed to the heat added by the lava. The heat that would be released from ambient water as it is cooled to 0 K is much larger than the heat added by the lava, explaining this discrepancy. Water velocity and flux values are consistent (within errors and reasonable temporal variation) between our study and those of Bonnefoy et al. (2019).

The main source of error in this calculation is in the water flux estimate, which was conducted with very crude field methods. In particular, the movement during acquisition of handheld video, and the inconsistent use of scales in the scenes, increased the uncertainties from  $<0.01 \text{ m s}^{-1}$  under ideal conditions to  $\sim0.05 \text{ m s}^{-1}$  in most of our measurements. In hindsight, the simple expedient of putting the camera on a tripod and leveling it with the horizon would have greatly reduced our uncertainties. However, because we used the average of several surface velocity measurements to estimate the water flux, we were able to derive useful estimates. By examining the stream profiles in detail, we were able to observe how velocities vary close to the bed and the banks. Most of the drop-off in velocity is in a relatively thin zone composing <<10% of the cross-sectional area of the stream. Thus, this velocity variability is minor if working to no more than two significant figures for the flux of water and heat, and a simple average of our velocity measurements excluding those shear zones does not introduce significant error.

We consider other possible sources of error in our heat flux estimates. Evaporative cooling may reduce the water temperature at the measurement locations relative to the value at the sources, but we confirmed that this effect was not large by comparing thermocouple measurements and thermal infrared imaging of the water surface. Side streams of unheated water make some contribution to the outflow. While these increase the water flux, they reduce the temperature, and should not affect the excess heat. Some inflows were even at temperatures slightly lower than the baseline. The observation of substantially cooler temperatures in the gravel centimeters below the base of warm streams implies that cooler water was flowing beneath the surface, and therefore that there is not much mixing between the cold subsurface water and the heated water at this location. However, this subsurface flow could have been heated to some degree; it was not possible to

**Table 1**2015 stream data for calculation of lava heating.

Stream	Cross-sectional Area (m²)	Mean Velocity (m s <sup>-1</sup> )	Excess T (°C) <sup>a</sup>
Inlet Stream 8/23b	2.8	2.9 <sup>c</sup>	_
Inlet Stream 8/24b	16	1.0 <sup>c</sup>	
Outflow 1	4.5	0.1 <sup>d</sup>	$4.5 \pm 3.0$
Outflow 2	0.5	0.34 <sup>d</sup>	$10.4 \pm 3.0$
Outflow 3	1.14	0.44 <sup>c</sup>	$22.2 \pm 3.0$
Outflow 4	0.63	0.66 <sup>c</sup>	$42.8 \pm 3.0$
Outflow 5	0.67	1.2 <sup>c</sup>	$40.8 \pm 3.0$
Outflow 6	4.12	0.37 <sup>c</sup>	$31.8 \pm 3.0$
Outflow 7	5.3	0.19 <sup>c</sup>	$18.6 \pm 3.0$

- <sup>a</sup> Above 5.6 °C baseline; see text.
- <sup>b</sup> Different but nearby cross-section locations.

measure the temperature without at least some disturbance that introduced warm water, so we do not have an accurate measurement of the water temperature below the streambed. Two significant uncertainties remain that we cannot quantify. The first is the amount of heat transported as steam from fumaroles and what fraction of that steam originated as rainwater versus subsurface sources. The second is the possibility that some subsurface water was heated but left the system via other pathways; much of the lava flow field is likely below the water table and the mobility of the water at depth is not well constrained. Clearly, the location is hydrologically complex, with high topography in several directions and a large preexisting groundwater spring just to the north of the lava terminus.

The most important uncertainty is the poor constraint on temporal variations from early in the cooling history when heat fluxes were the largest. Although we did not observe significant variations in the behavior of the hot springs on the days of in situ data collection, those data are limited temporal snapshots. At the same time, our observations of the changes to the southern lake in 2015, as well as the changes reported by Bonnefoy et al. (2019), suggest that variations in the hydrologic conditions surrounding the lava flow on various timescales were significant. Without continuous monitoring the uncertainties in the heat flux measurements cannot be fully characterized.

Our longer-term monitoring data provide some insights into those uncertainties and into the total heat loss. When data from times when the sensors were out of the water are excluded, most of the water temperature curves from 2016 to 2018 can be fit to reasonable accuracy by exponential curves with e-folding decay times of a few months to a few years. However, no single decay time works for all of the fits. Those curves are also a poor fit to measured temperatures from 2015 and to the complex variations that occurred in late 2016. This poses a challenge for definitively understanding how much energy was removed by the water. If we assume a linear decline from August 2014 (start of the eruption) to August 2017 (when the spring temperatures were barely above background) then aqueous advection removed  ${\sim}4\times10^{16}$  J. This history is obviously simplistic, but the data are not sufficient to enable more complex modeling. The total thermal energy that must be lost from the lava during cooling is  $\sim 5.3 \times 10^{18}$  J. This calculation assumes 1.21 km<sup>3</sup> of dense rock equivalent basaltic lava (Bonny et al., 2018), an eruption temperature of 1195 °C (Kolzenburg et al., 2017) cooling to 0 °C, a density of 2700 kg/m<sup>3</sup>, latent heat of crystallization of 400 kJ/kg (Keszthelyi, 1995), and temperature-dependent heat capacity following the Keszthelyi and Denlinger (1996) model for Hawaiian basalt. Neglecting crystallization, about  $3.6 \times 10^{17}$  J is lost during the emplacement phase, when the lava cooled from 1195 to 1095 °C (Kolzenburg et al., 2017). Thus, aqueous cooling by groundwater (as opposed to rain and snow falling on the flow) accounted for on the order of 1% of the total heat loss. However, because the water-enhanced cooling was localized, the process was more important near the lava terminus, with an effect multiplied by the inverse of the volume fraction of the lava that was water cooled. In the opposite end-member case, if the spring outflow water was heated only by the lava in the lower-bound area noted above (~1/40th of the flow area) then advection may have caused locally ~40% of the post-emplacement heat loss. The effect would be even higher because the lava is thinner than average near the terminus, but because the groundwater-cooled area is not well known an accurate calculation is not possible.

## 4. Discussion

## 4.1. Lava-water interaction

The hydrologic system at Holuhraun, defined here as the flow field and its interactions with surface runoff and subsurface flow, is controlled by groundwater rising from below or forced in from the side, closely coupled with surface flow arising from precipitation and glacial melt. The measurable aqueous cooling effect was thus affecting the

<sup>&</sup>lt;sup>c</sup> Measured by analysis of video. Formal uncertainty is difficult to quantify due to uneven spatial sampling of the streams and imperfect control of camera geometry. We estimated velocities via two independent feature-tracking methods with different approaches to handling the geometry and found them to generally agree to within 10%. The uncertainty is greater for the inlet stream on 8/23/2015 due to difficulty calibrating the geometry.

 $<sup>^{\</sup>rm d}$  Measured in the field; estimated accuracy  $\pm 25\%$ .

bottom of the lava flow. Inundation from above may be required for aqueous cooling to dominate, but greater hydraulic head could drive higher groundwater fluxes in conditions where lava interacts with steeper topography. If the end-member case where the water cooling was localized is accurate, this model could result in very important cooling effects even with low hydraulic head. Water pools were also observed on the lava surface at times, but their contribution to the cooling of the lava has not been determined.

In the Holuhraun system, at least some parts of the base of the massive flow core were persistently in contact with liquid water. Such a setting could produce conditions for the formation of orderly basal colonnade columnar jointing typified by relatively narrow columns at the base of the lava (e.g., Sæmundsson, 1970; Long and Wood, 1986; Goehring and Morris, 2008), depending on the stability and uniformity of the system. Parts of the flow core subjected to repeated and persistent contact with water could develop advection-dominated cooling. However, Goehring and Morris (2008) estimated heat fluxes of 200-2000 W m<sup>-2</sup> associated with several basal colonnades in the Columbia River Basalt Group. The low end of this range is similar to the upper-limit (minimum area) flux estimated above. Thus, a welldefined basal colonnade is unlikely in the Holuhraun lava except perhaps in places where the water flux was locally concentrated. However, this mechanism of aqueous cooling driven by groundwater rising from below may be applicable to the formation of some basal colonnades, especially in cases where the hydraulic head is stronger and forces more water into the lava. If ongoing fluvial erosion exposes the flow interior along the southern margin of the lava, it will be of interest to examine the jointing within the lava and look for effects of aqueous cooling, especially at locations where water was impounded. Hackly jointed entablature indicative of more intense water cooling (likely via inundation by flowing water) is unlikely in the 2014–2015 Holuhraun lavas.

#### 4.2. Implications for Mars

The lava flow from the 2014–2015 eruption at Holuhraun is in many ways a good analog for Martian lava flows, which often are interpreted to have been emplaced with high eruptive fluxes and rubble crusts (Keszthelyi et al., 2000, 2004, 2008; Pedersen et al., 2015). This style of aqueous cooling may also be important for Martian lava flows, which are likely to have flowed over and melted ice in many instances, producing hydrovolcanic features such as rootless cones (e.g., Squyres et al., 1987; Greeley and Fagents, 2001; Lanagan et al., 2001; Hamilton et al., 2010, 2011; Keszthelyi et al., 2010) and columnar joints (Milazzo et al., 2009). Many lavas on Mars occupy likely fluvial channels (e.g., Burr et al., 2002; Fuller and Head, 2002; Jaeger et al., 2007; Voigt and Hamilton, 2018) or have channels near their edges (e.g., Squyres et al., 1987). In some cases, lava may occupy older channels, or divert later, unrelated flows, and it can be difficult to discriminate between lava-formed and fluvially eroded channels. However, water and lava may possibly have emerged from the subsurface nearly simultaneously (e.g., Head et al., 2003), and/or lava may have melted ground ice to water that would subsequently drain downhill into lower parts of the flows. This could be an important part of the cooling history of Martian lava flows, which are potential targets for future exploration. Water flow also complicates simple models for heating water and ice at the base of lava flows (cf. Dundas and Keszthelyi, 2013). Moreover, warm water at the base of lava flows could form ephemeral oases for life, especially subsurface life that might be brought to the surface by aqueous floods.

## 4.3. Future field measurements and modeling

The aqueous cooling at the 2014–2015 Holuhraun flow field was only one example of lava–water interaction and more datasets would enable better characterization of such interactions. We were unable to begin systematic instrumental monitoring until ~17 months after the

conclusion of the eruption and did not reach a fully satisfactory set of procedures until the hydrothermal system had cooled to near ambient temperature. We have demonstrated in this work that significant insights can be derived from simple experiments and monitoring with a small number of low-cost sensors, but a larger number and earlier installation would have produced a more complete picture. Unfortunately, appropriate eruptions are not common. The sensor set will depend on the characteristics of the lava flow and local hydrology but must be sufficient to characterize each component of the inflow and outflow of water, ideally with multiple sensors each. For an eruption identical to the one in this study, our minimum sensor set would include at least seven sensors: one P-T sensor in the streambed near the vent, one in the lake on the northern margin, one in the Side Pool, one in the groundwater streams, two in the warm springs at the flow toe, and one in the glacial stream along the southern edge of the lava flow, as well as two sensors for weather logging. At least one or two additional sensors in each setting would be preferred to provide redundancy and assess spatial variability. One or more sensors to monitor the regional groundwater level would also be valuable but would require a different installation method than used here. Additionally, it would be desirable to revisit the site more often than yearly to adjust the sensor distribution in response to major changes in the hydrology. For instance, we would have instrumented the lake present in 2015 if we had sensors available at that time. Further insights would be gained by placing sensors in the ground immediately ahead of an advancing flow to gather data on the initial stage of cooling.

While the limitations of our dataset also limit our conclusions at this time, numerical modeling of the subsurface flow of water under the 2014–2015 Holuhraun flow field will likely reveal additional insights. Our data and the observations of Bonnefoy et al. (2019) provide constraints on the water flow and heating and their temporal variation, which can be used to constrain such modeling. Important features to reproduce include the timescale and temperatures of the late-stage cooling of the hydrothermal system, strong correlation in the depth variations of springs and pools, and evidence for weak diurnal variations in their outflow.

## **Declaration of Competing Interest**

The authors declare that they have no known competing financial interests or personal relationships that could have appeared to influence the work reported in this paper.

## Acknowledgements

All sensor data from 2016 to 2018 are available in Dundas et al. (2020). CMD was funded by a NASA Early Career Fellowship. Additional funding for LK and CMD was provided by NASA Solar System Workings agreement number 80HQTR18T0020. EL was funded by NSF grant numbers EAR-1250431 and EAR-1654588. MER was supported by a National Science Foundation postdoctoral fellowship No. EAR-1452748. CWH was funded by NASA Planetary Geology and Geophysics grant NNX14AL54G and the W. M. Keck Foundation. ÁH and TT were funded by Vinir Vatnajökulls. Scott Rowland, Greg Vaughan, and an anonymous reviewer provided helpful comments. We are grateful for field assistance by Rob Askew, Muhammad Aufaristama, Amber Keske, Andrew Ryan, Sarah Sutton, and Stephen Scheidt, and thank the other members of the 2015 field expedition for logistical coordination and outstanding teamwork. Gabriel Carrillo assisted with data analysis. Marc Hunter provided valuable assistance with the U.S. Geological Survey data release. The University of Iceland provided logistical assistance and valuable information about the eruption and conditions around the lava flow. Ulrich Münzer, Ludwig-Maximilians-University of Munich, Department for Earth and Environmental Sciences provided a UltraCam true orthophotomosaic (September 6, 2015) from the IsViews (Iceland subglacial Volcanoes interdisciplinary early warning system) project. We thank Vatnajökull National Park in Iceland for research permits, and the Drekagil rangers for information on local conditions. Any use of trade, firm, or product names is for descriptive purposes only and does not imply endorsement by the U.S. Government.

## Appendix A. Methods for sensor installation

This appendix expands on the best-practice methods that we determined for pressure/temperature sensor installation for the reference of others who may attempt similar studies. The measurement methods that we developed between 2015 and 2018 should allow rapid deployment of a useful low-cost sensor network that provides reliable monitoring of future fluvio-volcanic interactions or other events where similar data are desired, even in remote and sensitive locations.

The most significant challenge was the dynamic and vigorous nature of the hydrologic system. In quiet locations where the water flow was entirely sourced from groundwater, we found it sufficient to suspend sensors from a metal cable wrapped around protrusions (Fig. S2). In locations with more active flow and sedimentation, we constructed housings with 5 cm diameter PVC pipe to provide mechanical protection (Figs. S3, S4). This diameter left open space around the sensor, allowing the water level to adjust easily. Sensors were suspended from a cap at the top of the pipe, and the base remained open. To ensure that water could freely circulate in and out of the pipe and therefore accurately reflect the exterior water depth, short slits were cut in the side of the pipe at intervals. This effectively created a stilling well, necessary for accurate measurement of the water level in a fluvial setting. A hole was drilled in the cap in order to ensure that trapped air would not cause the pipe to become buoyant or interfere with the water depth measurement.

The pipes were cut in the field to a length appropriate to the particular site (0.5–1 m) and secured to outcrops with metal cable or wedged among rocks large enough to hold the apparatus in place (Fig. S4), depending on the setting. The latter approach was used in locations subject to high flow capable of displacing the pipe, as the large blocks were not subject to fluvial transport, and the pipes were also secured with loose fragments of cobble-sized lava. They were installed near vertically but precise vertical alignment was not necessary as this has no effect on the measurement of the water column pressure. These methods were visually unobtrusive and resulted in no damage to the environment after the sensors were removed.

One pernicious issue that we were unable to address was sedimentation in lacustrine settings. After discovering this issue when retrieving sensors in 2018, we considered designs with filters of thin mesh over the perforations in the pipe that could exclude silt-sized and larger particles but did not have the opportunity to deploy or test such an installation. As such, we do not have a demonstrated design that can continue to reliably measure water levels after being buried by sediment. It should be noted that while the lake sensor was buried by material that was mostly sand, the infill within the housing was densely packed silty mud, so it is necessary to exclude the finest suspended sediment without blocking water flow. The buried sensor returned to normal functionality after it was removed from the sediment-packed housing. In the future, the best mitigation for this challenge may be selecting sites that are not dead-end or backwater locations where deposition is likely.

In locations subject to active sedimentation or other rapid geomorphic change, photo documentation of the sensor location is necessary. Without such documentation readily available in the field, it would not have been possible to locate and recover the lake sensor in 2018 after burial.

Sensors rated for marine settings were appropriate for the conditions, and PVC pipes did not suffer appreciable degradation over the course of a year in this cool hydrothermal setting. Labels were waterproofed and affixed to sensors with packing tape and remained attached and undamaged. However, the sensors were suspended from outcrops or within housings using wire cable, which proved vulnerable

to corrosion. For sensors deployed in 2016 we initially used a thin cable, but this rusted through in several instances and resulted in the loss of one of the sensors. The housing of the Side Pool sensor lost in the winter of 2016–2017 remained in place, and the PVC pipe was likely displaced at high water after the cable had broken, allowing the sensor to slip out of the bottom of the housing and onto the streambed, where it was buried or carried downstream. A thicker, stainless steel cable with a flexible plastic coating (3 mm exterior diameter) proved much more robust and was in fair condition after one year of deployment, although it showed some signs of corrosion.

The simple weather sensors that we used were placed in sheltered locations and survived through the year. The weather sensor for 2016–2017 failed to collect valid pressure data and suffered from clock drift but it appears to have been inaccurate from the beginning of data collection rather than as a result of field conditions.

We did not encounter any issues with humans or animals tampering with or disturbing our sensors, although 1-cm step changes in water depth in the Toe Spring data were possibly caused by human activity. Although the remote setting of Holuhraun helped in this regard, the small size of the devices used made them easy to conceal from any casual observer.

## Appendix A. Supplementary data

Supplementary data to this article can be found online at https://doi.org/10.1016/j.jvolgeores.2020.107100.

#### References

- Baker, L.L., Bernard, A., Rember, W.C., Milazzo, M., Dundas, C.M., Abramov, O., Keszthelyi, L., 2015. Temperature profile around a basaltic sill intruded into wet sediments. J. Volc. Geotherm. Res. 302, 81–86. https://doi.org/10.1016/j.volgeores.2015.06.012.
- Bonnefoy, L.E., Hamilton, C.M., Scheidt, S.P., Duhamel, S., Höskuldsson, Á., Jónsdottir, I., Thordarson, T., Münzer, U., 2019. Landscape evolution associated with the 2014–2015 Holuhraun eruption in Iceland. J. Volc. Geotherm. Res. 387, 106652. https://doi.org/10.1016/j.jvolgeores.2019.07.019.
- Bonny, E., Thordarson, T., Wright, R., Höskuldsson, Á., Jónsdottir, I., 2018. The volume of lava erupted during the 2014 to 2015 eruption at Holuhraun, Iceland: a comparison between satellite- and ground-based measurements. J. Geophys. Res Solid Earth 123. 5412–5426. https://doi.org/10.1029/2017JB015008
- Burr, D.M., Grier, J.A., McEwen, A.S., Keszthelyi, L.P., 2002. Repeated aqueous flooding from the Cerberus Fossae: evidence for very recently extant, deep groundwater on Mars. Icarus 159, 53–73. https://doi.org/10.1006/icar.2002.6921.
- Dundas, C.M., Keszthelyi, L.P., 2013. Modeling steam pressure under Martian lava flows. Icarus 226, 1058–1067. https://doi.org/10.1016/j.icarus.2013.06.036.
- Dundas, C.M., Keszthelyi, L.P., Höskuldsson, Á., Thordarson, T., Hamilton, C.W., Lev, E., Rumpf, M.E., 2020. Sensor Data from Monitoring the Cooling of the 2014–2015 Lava Flow and Hydrothermal System at Holuhraun. Iceland. U.S, Geological Survey Data Release https://doi.org/10.5066/P9RMLJ7X.
- Fagents, S.A., Greeley, R., 2001. Factors influencing lava-substrate heat transfer and implications for thermomechanical erosion. Bull. Volcanol. 62, 519–532. https://doi.org/ 10.1007/s004450000113.
- Fagents, S.A., Thordarson, T., 2007. Rootless volcanic cones in Iceland and on Mars. In: Chapman, M.G. (Ed.), The Geology of Mars: Evidence from Earth-Based Analogs. Cambridge University Press, New York, pp. 151–177 https://doi.org/10.1017/CB09780511536014.007.
- Flynn, L.P., Mouginis-Mark, P.J., Horton, K.A., 1994. Distribution of thermal areas on an active lava flow field: Landsat observations of Kilauea, Hawaii, July 1991. Bull. Volcanol. 56, 284–296. https://doi.org/10.1007/BF00302081.
- Fuller, E.R., Head, J.W., 2002. Amazonis Planitia: the role of geologically recent volcanism and sedimentation in the formation of the smoothest plains on Mars. J. Geophys. Res. Planets 107, 5081. https://doi.org/10.1029/2002/E001842.
- Goehring, L., Morris, S.W., 2008. Scaling of columnar joints in basalt. J. Geophys. Res. 113, B10203. https://doi.org/10.1029/2007JB005018.
- Greeley, R., Fagents, S.A., 2001. Icelandic pseudocraters as analogs to some volcanic cones on Mars. J. Geophys. Res. 106, 20,527–20,546. https://doi.org/10.1029/2000JE001378.
- Hamilton, C.W., Fagents, S.A., Wilson, L., 2010. Explosive lava-water interactions in Elysium Planitia, Mars: Geologic and thermodynamic constraints on the formation of the Tartarus Colles cone groups. J. Geophys. Res. 115, E09006. https://doi.org/10.1029/2009|E003546.
- Hamilton, C.W., Fagents, S.A., Thordarson, T., 2011. Lava-ground ice interactions in Elysium Planitia, Mars: Geomorphological and geospatial analysis of the Tartarus Colles cone groups. J. Geophys. Res. 116, E03004. https://doi.org/10.1029/2010/E003657.
- Hamilton, C.W., Fitch, E.P., Fagents, S.A., Thordarson, T., 2017. Rootless tephra stratigraphy and emplacement processes. Bull. Volcanol. 79, 11. https://doi.org/10.1007/s00445-016-1086-4.

- Hardee, H.C., 1980. Solidification in Kilauea Iki lava lake. J. Volc. Geotherm. Res. 7, 211–223. https://doi.org/10.1016/0377-0273(80)90030-X.
- Hardee, H.C., 1982. Permeable convection above magma bodies. Tectonophysics 84, 179–195. https://doi.org/10.1016/0040-1951(82)90159-7.
- Harris, A.J., Rowland, S., 2001. FLOWGO: a kinematic thermo-rheological model for lava flowing in a channel. Bull. Volcanol. 63, 20–44. https://doi.org/10.1007/ s004450000120.
- Head, J.W., Wilson, L., Mitchell, K.L., 2003. Generation of recent massive floods at Cerberus Fossae, Mars by dike emplacement, cryospheric cracking, and confined aquifer groundwater release. Geophys. Res. Lett. 30, 1577. https://doi.org/10.1029/ 2003GL017135.
- Hildreth, W., Fierstein, J., 2012. The Novarupta-Katmai eruption of 1912—Largest eruption of the twentieth century: Centennial perspectives. U.S. Geological Survey Professional Paper 1791. 259 p. https://doi.org/10.3133/pp1791.
- Hon, K., Kauahikaua, J., Denlinger, R., Mackay, K., 1994. Emplacement and inflation of pahoehoe sheet flows: Observations and measurements of active lava flows on Kilauea Volcano. Hawaii. Geol. Soc. Am. Bull. 106, 351–370. https://doi.org/10.1130/ 0016-7606(1994)106<0351:EAIOPS>2.3CO;2.
- Jaeger, W.L., Keszthelyi, L.P., McEwen, A.S., Dundas, C.M., Russell, P.S., 2007. Athabasca Valles, Mars: a lava-draped channel system. Science 317, 1709–1711. https://doi. org/10.1126/science.1143315.
- Keszthelyi, L., 1995. Measurements of the cooling at the base of pahoehoe flows. Geophys. Res. Lett. 22, 2,195–2,198. https://doi.org/10.1029/95GL01812.
- Keszthelyi, L., Denlinger, R., 1996. The initial cooling of pahoehoe flow lobes. Bull. Volcanol. 58, 5–18. https://doi.org/10.1007/s004450050121.
- Keszthelyi, L., McEwen, A.S., Thordarson, T., 2000. Terrestrial analogs and thermal models for Martian flood lavas. J. Geophys. Res. 105, 15,027–15,049. https://doi.org/10.1029/ 1999IE001191.
- Keszthelyi, L., Harris, A.J.L., Dehn, J., 2003. Observations of the effect of wind on the cooling of active lava flows. Geophys. Res. Lett. 30, 1989. https://doi.org/10.1029/ 2003GI017994
- Keszthelyi, L., Thordarson, T., McEwen, A.S., Haack, H., Guilbaud, M.-N., Self, S., Rossi, M.J., 2004. Icelandic analogs to Martian flood lavas. Geochem. Geophys. Geosys. 5. https:// doi.org/10.1029/2004GC000758.
- Keszthelyi, L., Jaeger, W., McEwen, A., Tornabene, L., Beyer, R.A., Dundas, C., Milazzo, M., 2008. High Resolution Imaging Science Experiment (HiRISE) images of volcanic terrains from the first 6 months of the Mars Reconnaissance Orbiter primary Science phase. J. Geophys. Res. 113, E04005. https://doi.org/10.1029/2007JE002968.
- Keszthelyi, L.P., Jaeger, W.L., Dundas, C.M., Martínez-Alonso, S., McEwen, A.S., Milazzo, M.P., 2010. Hydrovolcanic features on Mars: preliminary observations from the first Mars year of HiRISE imaging. Icarus 205, 211–229. https://doi.org/10.1016/j.icarus.2009.08.020.
- Kolzenburg, S., Giordano, D., Thordarson, T., Höskuldsson, Á., Dingwell, D.B., 2017. The rheological evolution of the 2014/2015 eruption at Holuhraun, Central Iceland. Bull. Volcanol. 79, 45. https://doi.org/10.1007/s00445-017-1128-6.
- Lanagan, P.D., McEwen, A.S., Keszthelyi, L.P., Thordarson, T., 2001. Rootless cones on Mars indicating the presence of shallow equatorial ground ice in recent times. Geophys. Res. Lett. 28, 2,365–2,367. https://doi.org/10.1029/2001GL012932.
- Long, P.E., Wood, B.J., 1986. Structures, textures, and cooling histories of Columbia River basalt flows. GSA Bull. 97, 1144–1155. https://doi.org/10.1130/0016-7606(1986) 97<1144:STACHO>2.0.CO;2.
- Lorenz, V., 1973. On the formation of maars. Bull. Volcanol. 37, 183–204. https://doi.org/ 10.1007/BF02597130.

- MEPAG, 2020. Mars scientific goals, objectives, investigations, and priorities: 2020. D. Banfield, ed., 89 p. white paper posted March 2020 by the Mars Exploration Program Analysis Group (MEPAG) at. https://mepag.jpl.nasa.gov/reports.cfm.
- Milazzo, M.P., Keszthelyi, L.P., Jaeger, W.L., Rosiek, M., Mattson, S., Verba, C., Beyer, R.A., Geissler, P.E., McEwen, A.S., Team, HiRISE, 2009. Discovery of columnar jointing on Mars. Geology 37. 171–174. https://doi.org/10.1130/G25187A.1.
- Patrick, M.R., Dehn, J., Dean, K., 2004. Numerical modeling of lava flow cooling applied to the 1997 Okmok eruption: Approach and analysis. J. Geophys. Res. Solid Earth 109, B02210. https://doi.org/10.1029/2003/B002537.
- Pedersen, G.B.M., et al., 2015. Nornahraun lava morphology and emplacement: a new terrestrial analog for planetary lava flows. Lunar Planet. Sci. Conf. 46 abstract #1845.
- Pedersen, G.B.M., et al., 2017. Lava field evolution and emplacement dynamics of the 2014-2015 basaltic fissure eruption at Holuhraun. Iceland. J. Volc. Geotherm. Res. 340, 155–169. https://doi.org/10.1016/j.volgeores.2017.02.027.
- Rumpf, M.E., Fagents, S.A., Crawford, I.A., Joy, K.H., 2013. Numerical modeling of lavaregolith heat transfer on the Moon and implications for the preservation of implanted volatiles. J. Geophys. Res. Planets 118, 382–397. https://doi.org/10.1029/2012JE004131.
- Sæmundsson, K., 1970. Interglacial lava flows in the lowlands of southern Iceland and the problem of two-tiered columnar jointing. Jökull 20, 62–77.
- Sauer, V.B., Turnipseed, D.P., 2010. Stage measurement at gaging stations. U.S. Geological Survey Numbered Series Techniques and Methods 3-A7. https://doi.org/10.3133/ tm3A7
- Scheidt, S.P., Hamilton, C.W., 2019. Unmanned aerial system (UAS)-derived orthoimage mosaics and digital terrain models of the northeastern portion of the 2014–2015 Holuhraun lava flow-field, Iceland: Data acquired from 2015 to 2018. University of Arizona Spatial Data Explorer. https://doi.org/10.2458/azu\_geo\_holuhraun\_land-scape\_evolution.
- Sheridan, M.F., Wohletz, K.H., 1983. Hydrovolcanism: basic considerations and review. J. Volc. Geotherm. Res. 17, 1–29. https://doi.org/10.1016/0377-0273(83)90060-4.
- Sigmundsson, F., et al., 2015. Segmented lateral dyke growth in a rifting event at Bárðarbunga volcanic system, Iceland. Nature 517, 191–195. https://doi.org/ 10.1038/nature14111.
- Skilling, I.P., White, J.D.L., McPhie, J., 2002. Peperite: a review of magma-sediment mingling. J. Volc. Geotherm. Res. 114, 1–17. https://doi.org/10.1016/S0377-0273(01) 00278-5
- Squyres, S.W., Wilhelms, D.E., Moosman, A.C., 1987. Large-scale volcano-ground ice interactions on Mars. Icarus 70, 385–408. https://doi.org/10.1016/0019-1035(87) 90085-6.
- Thorarinsson, S., 1953. The crater groups in Iceland. Bull. Volcanol. 14, 3–44. https://doi.org/10.1007/BF02596003.
- Thordarson, T., Self, S., 1993. The Laki (Skaftár Fires) and Grímsvötn eruptions in 1783-1785. Bull. Volcanol. 55, 233–263. https://doi.org/10.1007/BF00624353.
- Turnipseed, D.P., Sauer, V.B., 2010. Discharge measurements at gaging stations. U.S. Geological Survey Numbered Series Techniques and Methods 3-A8. https://doi.org/10.3133/tm3A8.
- Voigt, J.R.C., Hamilton, C.W., 2018. Investigating the volcanic versus aqueous origin of the surficial deposits in Eastern Elysium Planitia. Mars. Icarus 309, 389–410. https://doi. org/10.1016/j.icarus.2018.03.009.